THE JOURNAL OF PHYSICAL CHEMISTRY LETTERS
A JOURNAL OF THE AMERICAN CHEMICAL SOCIETY

pubs.acs.org/JPCL

Letter

An H_2S-Regulated Artificial Nanochannel Fabricated by a Supramolecular Coordination Strategy

Huan Qin, Xiaolong Ding, Shi-Qi Cheng, Si-Yong Qin,* Xinya Han,* Yue Sun,* and Yi Liu

Cite This: *J. Phys. Chem. Lett.* 2022, 13, 9232−9237

Read Online

ACCESS | Metrics & More | Article Recommendations | Supporting Information

ABSTRACT: Hydrogen sulfide (H_2S), as the third gasotransmitter, has an important impact on physiological and pathological activities. Herein, we fabricated an artificial nanochannel with a conductance value of 2.01 nS via a supramolecular coordination strategy. Benefiting from the unique H_2S-mediated covalent reaction, the nanochannel biosensor could change from *ON* to *OFF* states with the addition of H_2S. Furthermore, this nanochannel directed the ion transport, showing a high rectification ratio as well as gating ratio. Subsequently, theoretical simulations were conducted to help to reveal the possible mechanism of the functionalized nanochannel. This study can provide insights for better understanding the process of H_2S-regulated biological channels and fabricating gas gated nanofluids.

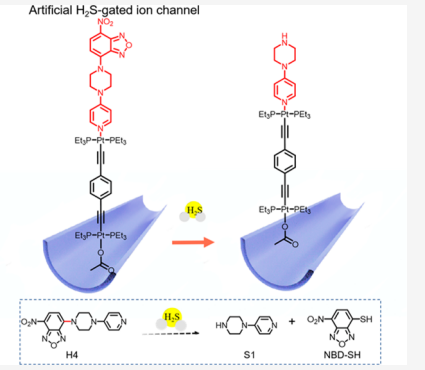

In response to endogenous stimuli, ion channels within membranes exhibit special transportation properties and therefore affect cell behaviors.[1−3] With inspiration from the abundant natural ion channels in biological systems, artificial intelligent nanochannels have attracted tremendous research attention in recent years.[4−6] Extensive research efforts have been announced toward the exploitation of novel stimuli to regulate the valves of channels.[7−10] To this end, the interfaces or internal walls of channels are decorated using different functional molecules to realize a specific response to environmental stimulation including pH,[11,12] temperature,[13,14] light,[15,16] and specific ions.[17,18] For example, Zhou and co-workers coated the anodized aluminum (AAO) with mesoporous carbon-silica (MCS) through an interfacial super-assembly strategy to construct a two-component MCS/AAO composite membrane, which exhibited enhanced permselectivity and could mediate the temperature and pH dual-sensitive ionic transport.[19] Despite the significant progress in external-stimuli-responsive nanochannels, examples of gas-responsive nanochannels are still rare.

Hydrogen sulfide (H_2S) is a kind of important gasotransmitter, which has an impact on extensive physiological and pathological activities, such as regulating myocardial contraction, vascular tone, and nerve conduction.[20−22] For example, H_2S has been found as a main regulator for calcium homeostasis within neurons, which activates Ca^{2+} to enter L-type Ca^{2+} channels, thus displaying neuronal activity. It also acts as an inhibitor of L-type calcium channels in cardiomyocytes to regulate cardiovascular functions.[23] Recently, H_2S has been documented to be capable of activating theATP-sensitive K^+ (KATP) channels in vascular smooth muscle cells, promoting vasodilation.[24] To comprehend the mechanism of H_2S in physiological systems, recently, researchers were devoted to constructing H_2S-responsive nanochannel biosensors.[25,26] Li and co-workers fabricated an artificial nanochannel biosensor with an outstanding H_2S response on the basis of an azide reduction reaction strategy.[27] Upon treatment with H_2S, the azido group immobilized on the nanochannel surface was reduced to an ammonium group, which then caused the aggregation of negative bovine serum albumin to inhibit K^+ transportation. Similar, fluorescent naphthalic anhydride azide was covalently located onto nanochannel arrays, to construct an H_2S-regulated system with a current signal and fluorescence response.[28] Despite the advancements, some problems remain to be solved. For instance, most of the reported responsive nanochannels are either according to the noncovalent interaction that may be sensitive to subtle interference[29] or based on step-by step covalent binding that needs a challenging synthesis.[30−33] Therefore, there is an urgent need to develop a simple, robust strategy to create artificial nanochannels to respond to H_2S.

Herein, we report a supramolecular coordination strategy to prepare an artificial H_2S-responsive nanochannel, and the H_2S-mediated covalent reaction was introduced to improve the specificity and stability toward H_2S (Figure 1). The 7-nitro-

Received: July 17, 2022
Accepted: September 9, 2022
Published: September 29, 2022

https://doi.org/10.1021/acs.jpclett.2c02233
J. Phys. Chem. Lett. 2022, 13, 9232−9237

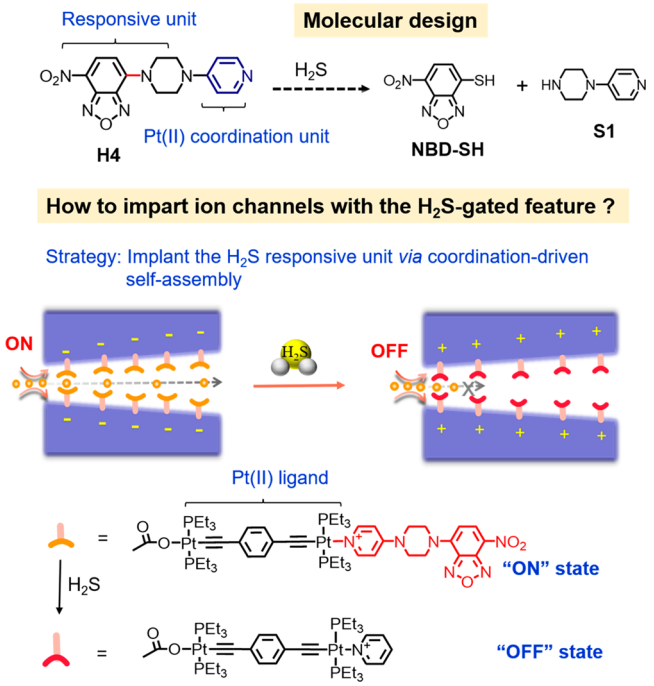

Figure 1. Schematic representation of modification process of an artificial nanochannel for the H_2S response based on a supramolecular coordination strategy. The system switched between *ON* and *OFF* states tuned by H_2S.

1,2,3-benzoxadiazole (NBD) amine was immobilized on the internal walls of nanochannels via a coordination strategy to construct an artificial ion gate.[34,35] In the presence of H_2S, H4 suffered from thiolysis, causing the reversion of surface charges from negative to positive to hinder ion transportation. Notably, the preparation of an H_2S-responsive nanochannel is simple without covalent modification and exhibits a good response, suggesting the efficiency for potential applications such as H_2S detection and modeling the H_2S-mediated biological channels.

Originating from the reactivity and selectivity toward H_2S, NBD amine 4-nitro-7-(4-pyridin-4-ylpiperazin-1-yl)-2,1,3-benzoxadiazole) (named H4) was introduced (Figure S1). ^{1}H NMR spectroscopy was used to characterize H4 (Figure S2). To investigate the H_2S-mediated response of a channel modified with H4, we first recorded the UV−vis absorption spectrum of piperidyl-based H4 with addition of micromolar H_2S. H4 solution showed an evident peak at 492 nm, in accordance with the absorbance of the NBD group (Figure S3). With the addition of H_2S (using Na_2S as an equivalent), the maximum absorption of solution exhibited a time-dependent redshift from 490 to 540 nm, which was ascribed to the generation of NBD-SH (Figure S4).[36] We further detected the UV absorption change of the H4 molecule in PBS buffer (pH 7.4, containing 2% DMSO, v/v) treated H_2S with different concentrations. Apparently, the increasing rate of absorbance at 540 nm was proportional to the concentration of H_2S (Figure S5). Meanwhile, we observed the fluorescence signal change of H4 solution after its incubation with 250 μM H_2S (Figure S6). The fluorescence of solution exhibited a downward trend, resulting from the generation of non-fluorescent 4-thiol-7-nitro-benzofurazan NBD-SH. Similarly, the higher concentration of H_2S, the faster the fluorescence signal declined (Figure S7).

According to an established method, we prepared a single conical artificial channel with a significant H_2S response using polyethylene terephthalate film[37] (Figure S8). As shown in the scanning electron microscopy (SEM, see Figure S9) image, the diameter of large opening was approximately 1290 nm, and the size of the tip was estimated by an electrochemical method to be 26.5 nm after asymmetrical etching. According to the zeta potential of the bare nanochannel, the bare nanochannel showed negative charge at different pHs (Figure S10). Notably, negative charges were attributed to carboxylate groups on the inner wall of the nanochannel, which could capture metal ligands by supramolecular coordination-driven self-assembly. As a consequence, the 180° Pt(II) ligand was selected as a bridge to immobilize H4 on the internal walls of nanochannels via a coordination strategy (Figure 2a).[38] The

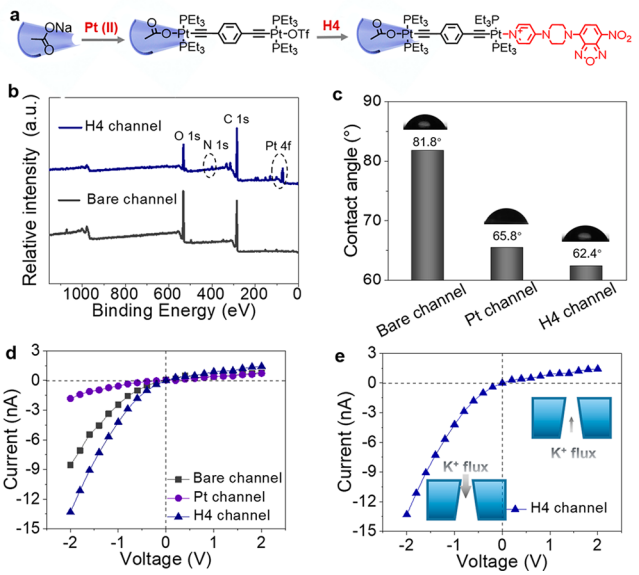

Figure 2. (a) Schematic representation for the fabrication of the functionalized H4 channel. (b) XPS spectra for the nanochannels before and after modification. (c) CA change of the different nanochannels. (d) *I*−*V* curves for the different channels in 0.1 M KCl. (e) *ON* state of the H4 channel for K^+ transport.

corresponding modification process can be confirmed via X-ray photoelectron spectroscopy (XPS) measurements. We found that only C 1s and O 1s signals were detected for bare channels (Figure 2b). In contrast, a new Pt4f and N1s peak appeared for the H4 channel, originating from the introduction of the Pt(II) ligand and H4 molecule. In addition, these modifications can be confirmed by the contact angle (CA) (Figure 2c). The chemical composition of nanochannels after modification displayed an evident change, leading to the varied wettability of the surface significantly from 81.8° to 65.8°, further to 62.4°.

In parallel, the K^+ transport property of the functionalized nanochannel was evaluated via the current−voltage (*I*−*V*) curves using a 0.1 M KCl electrolyte, and the *I*−*V* curves corresponding to different modification steps varied obviously (Figure 2d). Prior to the H4 modification, cation ions tended to transfer from the tip to the large opening via the rocking ratchet mechanism, which may be related to the deprotonation of the carboxyl group under neutral conditions. Meanwhile, under negative bias, the ionic current of this system increased rapidly due to the decrease of resistance. After the Pt(II) ligand immobilization on the nanochannels, the ionic current at −2 V

https://doi.org/10.1021/acs.jpclett.2c02233
J. Phys. Chem. Lett. 2022, 13, 9232−9237

declined from −8.57 to −1.83 nA, which is due to a close-to-neutral surface. After the subsequent introduction of the H4 molecular unit, the ion current increased remarkably to −13.3 nA (*ON* state, Figure 2e), which was ascribed to the significant increase of charge density as well as hydrophilicity.

Subsequently, we explored the response to H_2S of the nanochannels before and after modification. The K^+ transport property of the nanochannel was characterized using *I*−*V* measurements. Upon treatment with H_2S, the ion current of the bare nanochannel showed no apparent variation (Figure 3a), while the ion current at −2 V decreased distinctly for the

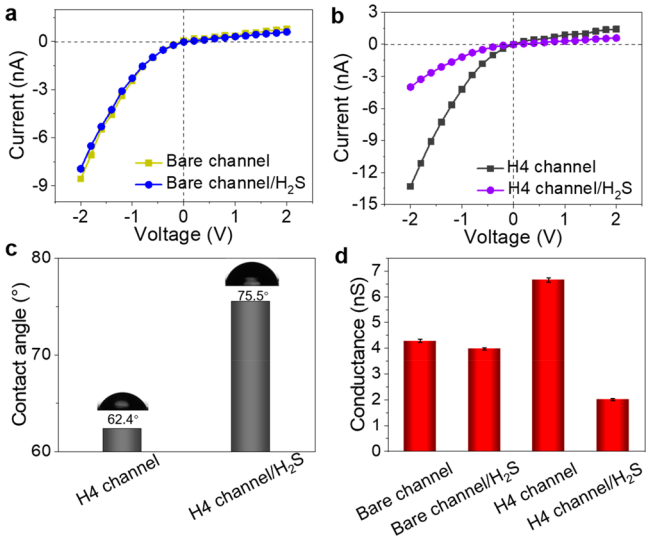

Figure 3. (a, b) *I*−*V* curves of the nanochannels toward H_2S stimuli. (c) CA change for the H4 nanochannel after incubation with H_2S. (d) Ion conductance of the bare and H4 channels before and after adding H_2S at −2 V.

H4 nanochannel (Figure 3b). The different ion current outputs for the modified nanochannel was attributed to the covalent reaction between the H4 molecule and H_2S, accompanied by the decrease of negative charge that led to the decreased surface charge density and increased hydrophobicity (Figure 3c). In the presence of H_2S, the H4 channel exhibited a low ion current and high resistance; namely, the gate exhibited the *OFF* state, impeding the transport of K^+. Furthermore, the conductance values (*G*) at −2 V for bare nanochannel, H4 nanochannel, bare nanochannel/H_2S, and H4 nanochannel/H_2S can be calculated as 4.28 nS, 6.65 nS, 3.97 nS, and 2.01 nS (Figure 3d), respectively, which further indicated the change of ion current.

The nanochannels showed evident ion current rectification due to the pore size asymmetries from the tip to base direction. The ion current rectification ratio is generally defined as $|I_{-2\ V}|/|I_{+2\ V}|$, where $|I_{-2\ V}|$ and $|I_{+2\ V}|$ are the absolute values of ion currents at a given voltage −2 V and +2 V, accordingly. As shown in Figure Figure 4a, after treating with H_2S, the ion current rectification ratio of the H4 channel varied from 13.2 to 6.9. Inspired by protein ion channels in the biological system, we found that the gating ratio of the artificial smart nanochannel could be remarkably enhanced by H_2S. To some degree, the gating ratio could reflect the effect of H_2S for K^+ transport within the nanochannels, which is calculated by $(I-I_0)/I_0$, where I_0 and *I* are the currents values at −2 V before and after addition of H_2S. The gating ratio was 0.7 for the

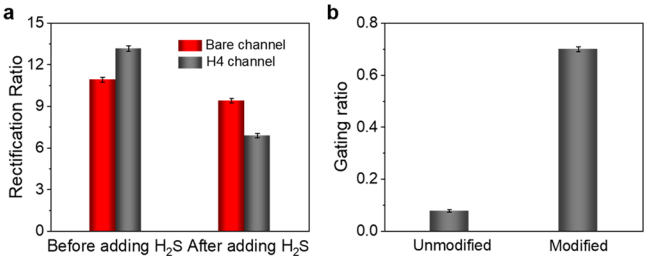

Figure 4. (a) H_2S-driven ionic current rectification. (b) H_2S-driven ion gating ratio (R_g).

nanochannel after the modification (*ON* state), which was much higher than the value of 0.08 for the bare nanochannel (Figure 4b). Meanwhile, increasing the concentration of H_2S, the ion current at −2 V decreased accompanied by a smaller rectification ratio (Figures S12 and 13). The phenomenon can be attributed to the fact that more H_2S molecules reacted with H4, which therefore led to the decrease of surface charge. To evaluate the time-dependent H_2S response of the nanochannel, we recorded the current change at different reaction times. The ion current gradually varied along with the increase in reaction time, showing the continuous reaction between the H4 molecule and H_2S with the increase of time (Figure S14). The ion current nearly no longer changed with the time up to 180 min, due to the reaction between the H4 molecule and H_2S approaching saturation.

To confirm the selectivity of the H4-modified functionalized nanochannel for H_2S, we treated the nanochannel with different substrates. The ionic current value at −2 V varied from −15.42 nA to −3.54 nA after adding H_2S (Figure S15). In contrast, the ion current shows little change with the addition of other substrates, which confirmed the high selectivity for H_2S of the H4 nanochannel. Moreover, the gating ratio of H_2S was remarkably higher than the values of other substrates, further indicating the selectivity of the H4 nanochannel for H_2S.

To probe the mechanism of the H_2S-regulated nanochannel biosensor switching between *ON* and *OFF* states, we quantitatively elucidated the characteristics of H_2S-activated nanochannels using theoretical simulations. The electro-osmotic flow (EOF) experiment was carried out to investigate the discrepancy in the charge density regulated by H_2S. Based on the Helmholtz-Smolucwski equation,[39,40] we found that the surface charge of the nanochannel before reacting with H_2S was negative (charge density −0.025 e nm^{-2}), but the latter channel was positively charged with a charge density of 0.009 e nm^{-2} (Figure 5a). In addition, we used zeta potential to confirm the change in surface charge of the H4 nanochannel toward H_2S stimuli (Figure S16). We found that the value of the zeta potential changed from negative to positive after adding H_2S, which is consistent with our theoretical simulation results.

The results indicated that H_2S could bind with the H4 molecule, resulting in the reversal of the negative surface charge. In addition, we employed COMSOL Multiphysics 5.5 to complete the finite element calculation on the basis of Poisson and Nernst−Planck (PNP) equations to explain the behavior of the functional nanochannels toward H_2S[41] based on the nanochannel model (Figure S17). The concentration distribution of two nanochannels at −2 V was shown in Figure 5b. Obviously, in the negatively charged nanochannel, the

https://doi.org/10.1021/acs.jpclett.2c02233
J. Phys. Chem. Lett. 2022, 13, 9232−9237

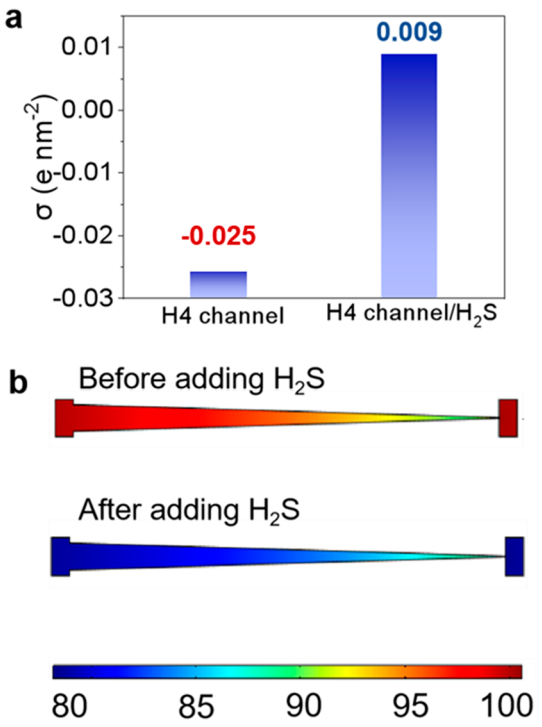

Figure 5. (a) The charge density comparison of the H4 channel toward H_2S stimuli. (b) The theoretical simulation of the ion concentration distribution profile comparison within the nanochannel (at −2 V, with 0.1 M KCl).

concentration of K^+ was much higher than that of the bulk solution. In contrast, K^+ depletion could be observed in the positively charged nanochannel. The K^+ enrichment in the negatively charged nanochannel was ascribed to the overlapped electric double layer (EDL) at the tip side, which further generated the concentration gradient, leading to the higher ion conductance and ionic current. These results can demonstrate the reversal ion gating mechanism of the H_2S-responsive nanochannel, which is attributed to surface charge regulation.

In conclusion, we successfully prepared an artificial H_2S-responsive biosensor. Relying on a supramolecular coordination strategy, the fabrication was simple with no need for covalent modification. Specifically, this nanochannel showed good H_2S-regulated gating and rectification performance, resulting from the unique thiolysis of H_2S-mediated H4. These experimental results will open up new ways to better understand the synergistic effects of H_2S messenger molecules in biological ion channels and further apply them in the fields of H_2S biosensors and detection.

■ ASSOCIATED CONTENT

Supporting Information

The Supporting Information is available free of charge at https://pubs.acs.org/doi/10.1021/acs.jpclett.2c02233.

^{1}H NMR spectrum of H4, UV−vis absorbance spectrum and fluorescence spectrum, materials source, experimental methods, SEM, *I*−*V* curve measurements, zeta potential, the model of numerical simulation (PDF)

Transparent Peer Review report available (PDF)

■ AUTHOR INFORMATION

Corresponding Authors

Yue Sun − *State Key Laboratory of Separation Membrane and Membrane Process & Tianjin Key Laboratory of Green Chemical Technology and Process Engineering, School of Chemistry, Tiangong University, Tianjin 300387, China;* orcid.org/0000-0002-6131-5706; Email: sunyue@tiangong.edu.cn

Si-Yong Qin − *Key Laboratory of Catalysis and Energy Materials Chemistry of Ministry of Education & Hubei Key Laboratory of Catalysis and Materials Science, South-Central University for Nationalities, Wuhan 430074, China;* orcid.org/0000-0001-5034-3309; Email: sy-qin@mail.scuec.edu.cn

Xinya Han − *School of Chemistry and Chemical Engineering, Anhui University of Technology, Anhui 243002, China;* Email: xinyahan@ahut.edu.cn

Authors

Huan Qin − *Key Laboratory of Catalysis and Energy Materials Chemistry of Ministry of Education & Hubei Key Laboratory of Catalysis and Materials Science, South-Central University for Nationalities, Wuhan 430074, China*

Xiaolong Ding − *School of Chemistry and Chemical Engineering, Anhui University of Technology, Anhui 243002, China*

Shi-Qi Cheng − *Key Laboratory of Catalysis and Energy Materials Chemistry of Ministry of Education & Hubei Key Laboratory of Catalysis and Materials Science, South-Central University for Nationalities, Wuhan 430074, China*

Yi Liu − *State Key Laboratory of Separation Membrane and Membrane Process & Tianjin Key Laboratory of Green Chemical Technology and Process Engineering, School of Chemistry, Tiangong University, Tianjin 300387, China; Hubei Key Laboratory of Radiation Chemistry and Functional Materials, Hubei University of Science and Technology, Xianning 437100, China;* orcid.org/0000-0001-7626-0026

Complete contact information is available at: https://pubs.acs.org/10.1021/acs.jpclett.2c02233

Author Contributions

H.Q., S.Q., X.H., and Y.S. designed the research; the manuscript was completed with contributions from all the authors.

Notes

The authors declare no competing financial interest.

■ ACKNOWLEDGMENTS

We are grateful to the National Key Research & Development Program (2019YFE0123100, 2021YFB3802200), the National Natural Science Foundation of China (82104065, 32061143045), and the Science and Technology Plans of Tianjin (21ZYJDJC00050).

■ REFERENCES

(1) Yang, J.; Yu, G.; Sessler, J. L.; Shin, I.; Gale, P. A.; Huang, F. Artificial Transmembrane Ion Transporters as Potential Therapeutics. *Chem.* **2021**, *7*, 3256−3291.

(2) Jayaram, A. K.; Pappa, A. M.; Ghosh, S.; Manzer, Z. A.; Traberg, W. C.; Knowles, T. P. J.; Daniel, S.; Owens, R. M. Biomembranes in Bioelectronic Sensing. *Trends. Biotechnol.* **2022**, *40*, 107−123.

(3) Feng, J.; Graf, M.; Liu, K.; Ovchinnikov, D.; Dumcenco, D.; Heiranian, M.; Nandigana, V.; Aluru, N. R.; Kis, A.; Radenovic, A. Single-Layer MoS_2 Nanopores as Nanopower Generators. *Nature* **2016**, *536*, 197−200.
(4) Hou, X.; Guo, W.; Jiang, L. Biomimetic Smart Nanopores and Nanochannels. *Chem. Soc. Rev.* **2011**, *40*, 2385−2401.
(5) Xiao, K.; Wen, L.; Jiang, L. Biomimetic Solid-State Nanochannels: from Fundamental Research to Practical Applications. *Small* **2016**, *12*, 2810−2831.
(6) Sun, Y.; Yi, F.; Li, R. H.; Min, X.; Qin, H.; Cheng, S. Q.; Liu, Y. Inorganic-Organic Hybrid Membrane Based on Pillararene-Intercalated MXene Nanosheets for Efficient Water Purification. *Angew. Chem., Int. Ed.* **2022**, *61*, No. e202200482.
(7) Jiang, Y.; Ma, W.; Qiao, Y.; Xue, Y.; Lu, J.; Gao, J.; Liu, N.; Wu, F.; Yu, P.; Jiang, L.; Mao, L. Metal-Organic Framework Membrane Nanopores as Biomimetic Photoresponsive Ion Channels and Photodriven Ion Pumps. *Angew. Chem., Int. Ed.* **2020**, *59*, 12795−12799.
(8) Sun, Y.; Chen, S.; Chen, X.; Xu, Y.; Zhang, S.; Ouyang, Q.; Yang, G.; Li, H. A Highly Selective and Recyclable NO-Responsive Nanochannel Based on a Spiroring Opening-Closing Reaction Strategy. *Nat. Commun.* **2019**, *10*, 1323.
(9) Cheng, M.; Zhu, F.; Zhang, S.; Zhang, X.; Dhinakaran, M. K.; Li, H. A Funnel-Shaped Chloride Nanochannel Inspired by ClC Protein. *Nano Lett.* **2021**, *21*, 4086−4091.
(10) Sun, Y.; Zhang, F.; Quan, J.; Zhu, F.; Hong, W.; Ma, J.; Pang, H.; Sun, Y.; Tian, D.; Li, H. A Biomimetic Chiral-Driven Ionic Gate Constructed by Pillar[6]arene-Based Host-Guest Systems. *Nat. Commun.* **2018**, *9*, 2617.
(11) Sun, Z.; Han, C.; Wen, L.; Tian, D.; Li, H.; Jiang, L. pH Gated Glucose Responsive Biomimetic Single Nanochannels. *Chem. Commun.* **2012**, *48*, 3282−3284.
(12) Lin, T. W.; Hsu, J. P. Pressure-Driven Energy Conversion of Conical Nanochannels: Anomalous Dependence of Power Generated and Efficiency on pH. *J. Colloid Interface Sci.* **2020**, *564*, 491−498.
(13) Wang, R.; Sun, Y.; Zhang, F.; Song, M.; Tian, D.; Li, H. Biomimetic Temperature-Gated 2D Cationic Nanochannels for Controllable Osmotic Power Harvesting. *Angew. Chem., Int. Ed.* **2017**, *56*, 5294−5298.
(14) Wu, C.; Xiao, T.; Tang, J.; Zhang, Q.; Liu, Z.; Liu, J.; Wang, H. Temperature-Sensitive Artificial Channels through Pillar[5]arene-Based Host-Guest Interactions. *Nano Energy* **2020**, *76*, 105−113.
(15) Sun, Y.; Ma, J.; Zhang, F.; Zhu, F.; Mei, Y.; Liu, L.; Tian, D.; Li, H. A Light-Regulated Host-Guest-Based Nanochannel System Inspired by Channelrhodopsins Protein. *Nat. Commun.* **2017**, *8*, 260.
(16) Wen, L.; Liu, Q.; Ma, J.; Tian, Y.; Li, C.; Bo, Z.; Jiang, L. Malachite Green Derivative-Functionalized Single Nanochannel: Light-and-pH Dual-Driven Ionic Gating. *Adv. Mater.* **2012**, *24*, 6193−6198.
(17) Liu, Q.; Xiao, K.; Wen, L.; Dong, Y.; Xie, G.; Zhang, Z.; Bo, Z.; Jiang, L. A Fluoride-Driven Ionic Gate Based on a 4-Aminophenylboronic Acid-Functionalized Asymmetric Single Nanochannel. *ACS Nano* **2014**, *8*, 12292−12299.
(18) Chen, W.; Dong, T.; Xiang, Y.; Qian, Y.; Zhao, X.; Xin, W.; Kong, X. Y.; Jiang, L.; Wen, L. Ionic Crosslinking-Induced Nanochannels: Nanophase Separation for Ion Transport Promotion. *Adv. Mater.* **2022**, *34*, 2108410.
(19) Zhou, S.; Xie, L.; Li, X.; Huang, Y.; Zhang, L.; Liang, Q.; Yan, M.; Zeng, J.; Qiu, B.; Liu, T.; Tang, J.; Wen, L.; Jiang, L.; Kong, B. Interfacial Super-Assembly of Ordered Mesoporous Carbon-Silica/AAO Hybrid Membrane with Enhanced Permselectivity for Temperature- and pH-Sensitive Smart Ion Transport. *Angew. Chem., Int. Ed.* **2021**, *60*, 26167−26176.
(20) Ma, Y.; Li, X.; Li, A.; Yang, P.; Zhang, C.; Tang, B. H_2S-Activable MOF Nanoparticle Photosensitizer for Effective Photodynamic Therapy against Cancer with Controllable Singlet-Oxygen Release. *Angew. Chem., Int. Ed.* **2017**, *56*, 13752−13756.
(21) Wu, L.; Sun, Y.; Sugimoto, K.; Luo, Z.; Ishigaki, Y.; Pu, K.; Suzuki, T.; Chen, H. Y.; Ye, D. Engineering of Electrochromic Materials as Activatable Probes for Molecular Imaging and Photodynamic Therapy. *J. Am. Chem. Soc.* **2018**, *140*, 16340−16352.
(22) Shukla, P.; Khodade, V. S.; SharathChandra, M.; Chauhan, P.; Mishra, S.; Siddaramappa, S.; Pradeep, B. E.; Singh, A.; Chakrapani, H. On Demand" Redox Buffering by H_2S Contributes to Antibiotic Resistance Revealed by a Bacteria-Specific H_2S Donor. *Chem. Sci.* **2017**, *8*, 4967−4972.
(23) Liu, X.; Zhang, N.; Ding, Y.; Cao, D.; Huang, Y.; Chen, X.; Wang, R.; Lu, N. Hydrogen Sulfide Regulates the [$Ca^{(2+)}$]i Level in the Primary Medullary Neurons. *Oxidative Med. Cell. Longev.* **2016**, *2016*, 2735347.
(24) Teng, X.; Li, H.; Xue, H.; Jin, S.; Xiao, L.; Guo, Q.; Wu, Y. GABAA Receptor, KATP Channel and L-type Ca^{2+} Channel is Associated with Facilitation Effect of H_2S on the Baroreceptor Reflex in Spontaneous Hypertensive Rats. *Pharmacol. Rep.* **2019**, *71*, 968−975.
(25) Guo, J.; Yang, L.; Xu, H.; Zhao, C.; Dai, Z.; Gao, Z.; Song, Y. Y. Biomineralization-Driven Ion Gate in TiO_2 Nanochannel Arrays for Cell H_2S Sensing. *Anal. Chem.* **2019**, *91*, 13746−13751.
(26) He, H.; Zhao, C.; Xu, J.; Qu, K.; Jiang, Z.; Gao, Z.; Song, Y. Y. Exploiting Free Standing P-CuO/n-TiO_2 Nanochannels as a Flexible Gas Sensor with High Sensitivity for H_2S at Room Temperature. *ACS Sens.* **2021**, *6*, 3387−3397.
(27) Zhang, R.; Chen, X.; Sun, Z.; Chen, S.; Gao, J.; Sun, Y.; Li, H. Switchable Nanochannel Biosensor for H_2S Detection Based on an Azide Reduction Reaction Controlled BSA Aggregation. *Anal. Chem.* **2019**, *91*, 6149−6154.
(28) Wu, I.; Zhang, D.; Zhang, X. A Facile Strategy for the Ion Current and Fluorescence Dual-Lock in Detection: Naphthalic Anhydride Azide (NAA)-Modified Biomimetic Nanochannel Sensor towards H_2S. *Chemosensors* **2021**, *9*, 298.
(29) Xu, Y.; Sui, X.; Jiang, J.; Zhai, J.; Gao, L. Ion Nanochannels: Smooth Muscle Cell-Mimetic CO-Regulated Ion Nanochannels. *Adv. Mater.* **2016**, *28*, 10780−10785.
(30) Cheng, S.; Liu, X.; Han, Z.; Rong, Y.; Qin, S.; Sun, Y.; Li, H. Tailoring CO_2-Activated Ion Nanochannels Using Macrocyclic Pillararenes. *ACS Appl. Mater. Interfaces.* **2021**, *13*, 27255−27261.
(31) Guo, J.; Yang, L.; Gao, Z.; Zhao, C.; Mei, Y.; Song, Y. Y. Insight of MOF Environment-Dependent Enzyme Activity via MOFs-in-Nanochannels Configuration. *ACS Catal.* **2020**, *10*, 5949−5958.
(32) Xu, J.; Xue, Y.; Jian, X.; Zhao, Y.; Dai, Z.; Xu, J.; Gao, Z.; Mei, Y.; Song, Y. Y. Understanding of Chiral Site-Dependent Enantioselective Identification on a Plasmon-Free Semiconductor Based SERS Substrate. *Chem. Sci.* **2022**, *13*, 6550−6557.
(33) Qu, K.; Xu, J.; Xue, Y.; Guo, J.; Gao, Z.; Song, Y. Y.; Mei, Y. Near Infrared Light-Driven Photothermal Effect on Homochiral Au/TiO_2 Nanotube Arrays for Enantioselective Desorption. *Anal. Chem.* **2022**, *94*, 588−592.
(34) Song, F.; Li, Z.; Li, J.; Wu, S.; Qiu, X.; Xi, Z.; Yi, L. Investigation of Thiolysis of NBD Amines for the Development of H_2S Probes and Evaluating the Stability of NBD Dyes. *Org. Biomol. Chem.* **2016**, *14*, 11117−11124.
(35) Ismail, I.; Chen, Z.; Sun, L.; Ji, X.; Ye, H.; Kang, X.; Huang, H.; Song, H.; Bolton, S. G.; Xi, Z.; Pluth, M. D.; Yi, L. Highly Efficient H_2S Scavengers via Thiolysis of Positively-Charged NBD Amines. *Chem. Sci.* **2020**, *11*, 7823−7828.
(36) Montoya, L. A.; Pearce, T. F.; Hansen, R. J.; Zakharov, L. N.; Pluth, M. D. Development of Selective Colorimetric Probes for Hydrogen Sulfide Based on NucleoPphilic Aromatic Substitution. *J. Org. Chem.* **2013**, *78*, 6550−6557.
(37) Jiang, Y.; Liu, N.; Guo, W.; Xia, F.; Jiang, L. Highly-Efficient Gating of Solid-State Nanochannels by DNA Supersandwich Structure Containing ATP Aptamers: A Nanofluidic Implication Logic Device. *J. Am. Chem. Soc.* **2012**, *134*, 15395−15401.
(38) Chakrabarty, R.; Mukherjee, P. S.; Stang, P. J. Supramolecular Coordination: Self-Assembly of Finite Two- and Three-Dimensional Ensembles. *Chem. Rev.* **2011**, *111*, 6810−6918.
(39) Xiao, K.; Xie, G.; Zhang, Z.; Kong, X.-Y.; Liu, Q.; Li, P.; Wen, L.; Jiang, L. Enhanced Stability and Controllability of an Ionic Diode

https://doi.org/10.1021/acs.jpclett.2c02233
J. Phys. Chem. Lett. 2022, 13, 9232−9237

Based on Funnel-Shaped Nanochannels with an Extended Critical Region. *Adv. Mater.* **2016**, *28*, 3345−3350.
(40) Jin, P.; Mukaibo, H.; Horne, L. P.; Bishop, G. W.; Martin, C. R. Electroosmotic Flow Rectification in Pyramidal-Pore Mica Membranes. *J. Am. Chem. Soc.* **2010**, *132*, 2118−2119.
(41) Zhang, Q.; Zhang, Z.; Zhou, H.; Xie, Z.; Wen, L.; Liu, Z.; Zhai, J.; Diao, X. Redox Switch of Ionic Transport in Conductive Polypyrrole-Engineered Unipolar Nanofluidic Diodes. *Nano Research* **2017**, *10*, 3715−3725.

https://doi.org/10.1021/acs.jpclett.2c02233
J. Phys. Chem. Lett. 2022, 13, 9232−9237